Thermal quenching of chromium photoluminescence in ordered perovskites. I. Temperature dependence of spectra and lifetimes

L. J. Andrews, A. Lempicki,* B. C. McCollum, and C. J. Giunta†

GTE Laboratories, Inc., Waltham, Massachusetts 02254

R. H. Bartram and J. F. Dolan

Department of Physics and Institute of Materials Science, University of Connecticut, Storrs, Connecticut 06268

The temperature dependence of chromium photoluminescence spectra and lifetimes have been measured in ordered perovskite (Cs_2NaYCl_6, K_2NaScF_6, and K_2NaGaF_6) host crystals. Analysis of lifetime data yields thermal-quenching activation energies ΔE of 4250, 7270, and 9240 cm^{-1}, respectively. The Mott theory, applied to a single-configuration-coordinate, linear-coupling model with parameters inferred from emission spectra, fails by 20 orders of magnitude to explain the observed radiationless-transition rate.

I. INTRODUCTION

Low-field chromium complexes are characterized by broadband $^4T_{2g} \rightarrow {}^4A_{2g}$ fluorescence, in contrast with the narrow-band $^2E_g \rightarrow {}^4A_{2g}$ phosphorescence of high-field complexes, such as ruby.[1] The distinction between low- and high-field complexes is illustrated by the energy-level diagram[2] shown in Fig. 1. Potential applications to tunable lasers[3] make it imperative to achieve a fundamental understanding of the factors which govern quantum efficiency of fluorescence in these materials. The present investigation was initiated with that objective.
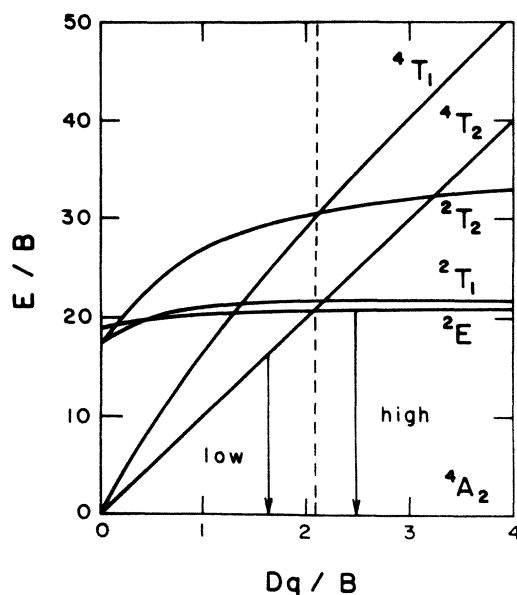
Low-field host materials include a variety of glasses[4]

FIG. 1. Tanabe-Sugano energy-level diagram for a d^3 configuration in octahedral symmetry, for the case $C/B = 4.50$. The vertical dashed line separates high-field and low-field complexes.

and single crystals.[3] Thermal quenching of fluorescence is found to be strongly host dependent, and to be surprisingly sensitive to constituents beyond the immediate ligands. Similar behavior has been reported for V^{2+} in MgF_2, MnF_2, and $KMgF_3$.[5]

The host materials selected for the present investigation have ordered perovskite (elpasolite) crystal structure, with formula A_2BMX_6, where A and B are monovalent cations, M is a trivalent cation, and X is a monovalent anion. These host crystals have the virtue that they can accommodate a trivalent cation impurity, such as Cr^{3+}, at a rigorously octahedral site without charge compensation. Three such compounds which exhibit disparate luminescence behavior were investigated extensively; these include K_2NaScF_6:Cr^{3+} and K_2NaGaF_6:Cr^{3+}, which fluoresce efficiently at room temperature, and Cs_2NaYCl_6:Cr^{3+}, which does not. The two fluoride compounds lie near the boundary between low-field and high-field complexes while the chloride compound is well on the low-field side.

The temperature dependence of fluorescence lifetime has been measured, and correlated with relative intensity, in order to characterize the thermal quenching of fluorescence. An independent characterization of electron-lattice interaction is achieved by analysis of the temperature dependence of fluorescence spectra.

Experimental techniques are described in Sec. II, and the temperature dependence of fluorescence lifetimes is reported in Sec. III. Fluorescence and absorption spectra are presented in Sec. IV. These data are interpreted in terms of a single-configuration-coordinate model in Sec. V. A more comprehensive theoretical description is developed in paper II.[6]

II. EXPERIMENTAL TECHNIQUES

Samples were prepared by mixing stoichiometric proportions of starting materials, in the form of powders of the halides of each cation, in an argon glove box. Mixtures were heated above the melting point in sealed tubes (quartz for the chloride and platinum for the fluorides), and allowed to cool slowly. The resulting samples were

polycrystalline, with occasional single crystals of sufficient clarity for absorption measurements. X-ray diffraction powder patterns were obtained in order to verify successful formation of the elpasolite structure. In one case, that of $K_2NaScF_6:Cr^{3+}$, the precise octahedral site symmetry of the chromium ion was verified by means of an electron-spin-resonance spectrum measured at room temperature, which consisted of a single line of width 25 G at $g = 1.97$.[7]

Fluorescence lifetimes were measured with 5-nsec pulsed excitation at 5800 Å by a Lambda Physik nitrogen-laser-pumped dye laser. Peak luminescence was isolated by means of a Spex 1404 monochrometer, and detected with a cooled S1 photomultiplier (ITT FW118 or RCA 7102). Photon counting was accomplished with a PRA 1762 amplifier-discriminator and a Nicolet 1170 multichannel scalar which can be swept at 1 μsec per channel. The decays were observed to be exponential over three decades. Fluorescence lineshapes were measured using cw excitation from a Krypton-ion laser at 5682 Å, the Spex monochrometer, and either the cooled RCA 7102 photomultiplier (for fluorides) or a North coast cooled GE detector (for the chloride). The detection system response was calibrated with a standard 1-KW tungsten-halogen lamp which was calibrated against a National Bureau of Standards (NBS) standard lamp, in order to correct spectral data. Measurements below room temperature were made by flowing cooled nitrogen gas past the sample in a quartz Dewar, and measurements above room temperature were made in a resistance-heated furnace with a Pyrex window. Temperatures were measured with an iron-constantin thermocouple in close proximity with the sample, and in all cases were controlled within 2 °C. Both fluorescence lifetime and spectral data were stored in a Data General Eclipse S/120 minicomputer for subsequent analysis. Absorption spectra were measured on irregular single-crystal samples with a Cary 17 spectrophotometer.

III. FLUORESCENCE LIFETIMES

Fluorescence lifetimes τ were measured as a function of temperature between 4 and 700 K, and are plotted in Fig. 2. The transition rate is given by

$$\tau^{-1} = \tau_R^{-1} + \tau_{NR}^{-1} , \tag{1}$$

where τ_R^{-1} is the radiative rate and τ_{NR}^{-1} is the nonradiative rate. Two distinct trends are evident in the data for each compound, with a fairly abrupt transition between them. Radiative transitions dominate at lower temperatures, and the slow decline of τ with increasing temperature is attributed in part to thermal enhancement of phonon-assisted transitions, and in part to the proximity of the ^2E_g and $^4T_{2g}$ states in these materials. This interpretation is supported by the measured quantum efficiency of fluorescence of $K_2NaScF_6:Cr^{3+}$, which is essentially 100% at room temperature.[3] The much more rapid decline of τ at higher temperatures is well correlated with diminishing fluorescence intensity, as shown in Fig. 3, and is accordingly attributed to the dominance of nonradiative transitions. The respective rates can be fitted over a limited temperature range to expressions of the form
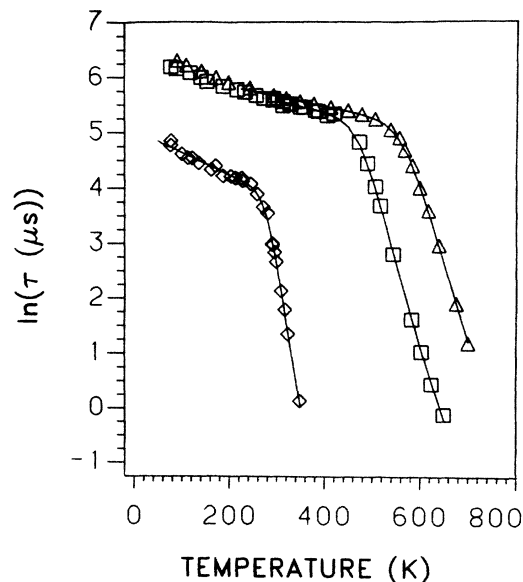

FIG. 2. Fluorescence lifetimes versus temperature for substitutional Cr^{3+} in Cs_2NaYCl_6 ($\Diamond$), K_2NaScF_6 ($\Box$), and K_2NaGaF_6 ($\triangle$). Solid lines are least-squares fits to Eqs. (1)–(3), over the indicated temperature ranges.

$$\tau_R^{-1} = \tau_0^{-1} \exp(\alpha T) , \tag{2}$$

$$\tau_{NR}^{-1} = s \exp(-\Delta E / k_B T) . \tag{3}$$

The exponential form for τ_R^{-1} is strictly empirical, and provides a convenient form for extrapolation to higher temperatures in order to facilitate extraction of the nonradiative rate, τ_{NR}^{-1}. The parameters s and ΔE are listed in Table I. The frequency factor s and activation energy ΔE provide a convenient way of summarizing data in the tem-
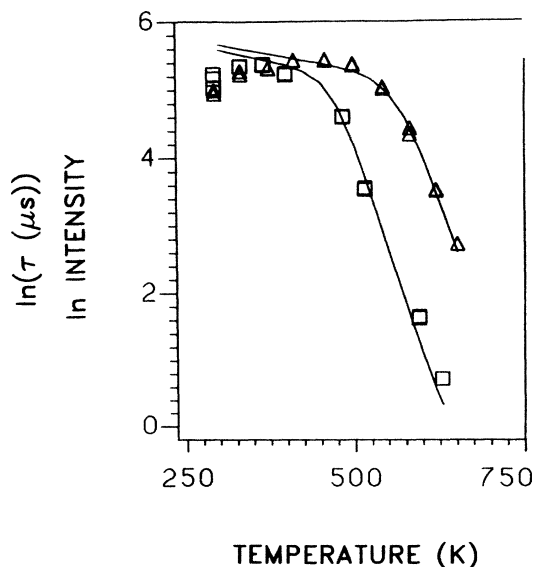

FIG. 3. Comparison of fluorescence lifetimes (solid lines) with integrated intensity (symbols) for K_2NaScF_6 ($\Box$) and K_2NaGaF_6 ($\triangle$).

TABLE I. Frequency factor s and activation energy ΔE for thermal quenching of Cr^{3+} fluorescence, inferred from the temperature dependence of fluorescence lifetimes.

Host crystal	s (10^{13} sec^{-1})	ΔE (cm^{-1})
Cs_2NaYCl_6	3.8	4250
K_2NaScF_6	1.2	7270
K_2NaGaF_6	5.2	9240

perature range of interest, and the empirical values of s are the signature of a first-order kinetic process; however, the interpretation of these parameters in terms of the theory of nonradiative transitions is fairly subtle, as will be evident from II.[6]

IV. OPTICAL SPECTRA

Several spectroscopic investigations of Cr^{3+} in crystals of elpasolite structure have been performed at liquid-He temperature,[8–12] and resolved vibronic structure of both absorption and photoluminescence spectra has been interpreted in terms of specific modes of vibration. Materials investigated include Cs_2NaYCl_6:Cr^{3+},[8] $Cs_2NaInCl_6$:Cr^{3+},[9] K_2NaCrF_6,[10,11] K_2NaGaF_6:Cr^{3+},[11,12] and K_2NaAlF_6:Cr^{3+}.[12] In the present investigation, featureless spectra were investigated at higher temperatures, in order to provide a more direct characterization of electron-lattice coupling by moments analysis.[13] In principle, the same information can be derived by deconvolution of resolved low-temperature spectra.[14]

Fluorescence spectra were recorded for the chloride elpasolite in the temperature range 77—300 K, and for both fluorides in the range 300—700 K. Typical spectra are shown in Fig. 4. First and second moments of these spectra were calculated at each temperature from the relations
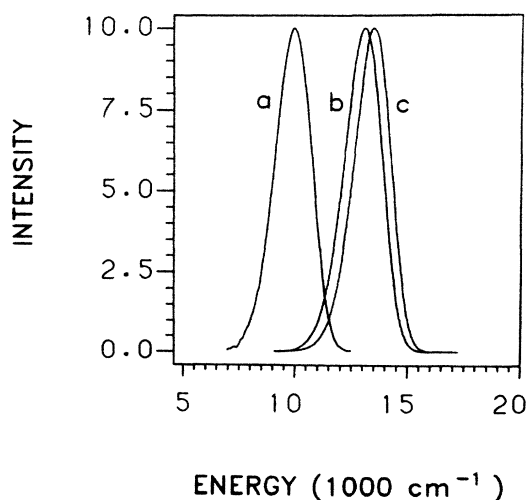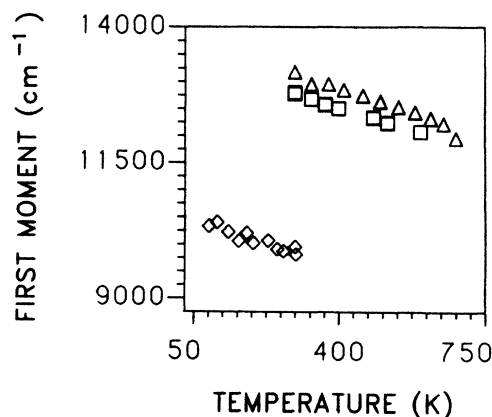

FIG. 5. Temperature dependence of the first moments of chromium fluorescence spectra in Cs_2NaYCl_6 ($\Diamond$), K_2NaScF_6 ($\square$), and K_2NaGaF_6 ($\triangle$).

$$N_1 = \langle E \rangle , \tag{4}$$

$$N_2 = \langle (E - \langle E \rangle)^2 \rangle , \tag{5}$$

$$\langle f(E) \rangle = \int_{-\infty}^{\infty} dE\, f(E) I(E) , \tag{6}$$

where E is the photon energy and and $I(E)$ is a normalized line-shape function such that $EI(E)$ is proportional to the corrected photon count rate per unit energy range. These moments are plotted as functions of temperature in Figs. 5 and 6, respectively.

The room-temperature optical absorption spectra of K_2NaScF_6:Cr^{3+} and K_2NaGaF_6:Cr^{3+} have been reported previously.[3,11] The absorption spectrum of Cs_2NaYCl_6:Cr^{3+} was measured in the present investigation. Peak positions are listed in Table II, together with inferred values of the crystal-field parameter Dq and the Racah parameters B and C/B.
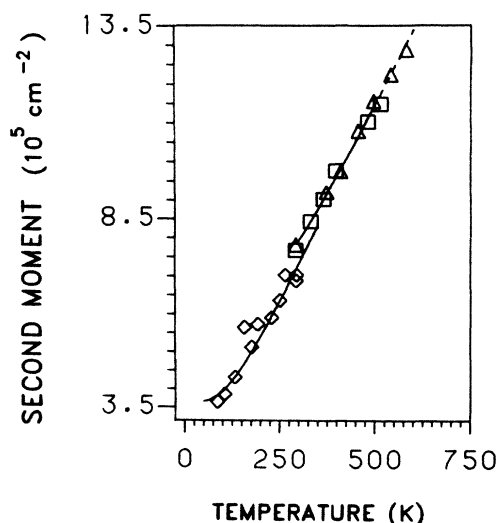

FIG. 4. Corrected fluorescence spectra at 300 K for (a) Cs_2NaYCl_6:Cr^{3+}, (b) K_2NaScF_6:Cr^{3+}, and (c) K_2NaGaF_6:Cr^{3+}.

FIG. 6. Temperature dependence of the second moments of chromium fluorescence spectra in Cs_2NaYCl_6 ($\Diamond$), K_2NaScF_6 ($\square$), and K_2NaGaF_6 ($\triangle$).

TABLE II. Peak positions (nm) from room-temperature optical absorption spectra of Cr^{3+} in ordered perovskites. The crystal-field parameter Dq and Racah parameters B and C (cm^{-1}) were determined by diagonalizing Tanabe-Sugano matrices and fitting to observed spectra [see S. Sugano, Y. Tanabe, and H. Kamimura, *Multiplets of Transition-Metal Ions in Crystals* (Academic, New York, 1970), p. 296]. Values in parentheses were inferred from low-temperature spectra.

Final state	Cs_2NaYCl_6	K_2NaScF_6[a]	K_2NaGaF_6[b]
$^4T_2$	790	641	625
$^4T_1(a)$	555	435	429
^2E	687	650	647
$^2T_1$	660	613	608
$^2T_2$	495	445	
$^4T_1(b)$		280	
Dq	1266 (1280)[c]	1560	1600
B	547 (600)[c]	794	771
C/B	6.40 (5.25)[c]	4.07	4.30

[a]P. T. Kenyon, L. Andrews, B. McCollum, and A. Lempicki, IEEE J. Quantum Electron. QE-18, 1189 (1982).
[b]J. Ferguson, H. J. Guggenheim, and D. L. Wood, J. Chem. Phys. 54, 504 (1971), Fig. 2.
[c]R. W. Schwartz, Inorg. Chem. 15, 2817 (1976).

V. DISCUSSION

Measurements of fluorescence lifetimes yield activation energies for the competing nonradiative processes which diminish fluorescence quantum efficiency. Within the context of a specific model, the parameters which characterize electron-lattice coupling can be inferred from the temperature dependence of fluorescence spectra. These parameters provide a basis for quantitative theoretical predictions of radiationless transition rates in II.[6] The present discussion is confined to interpretation in terms of a single-configuration-coordinate, linear-coupling model, illustrated in Fig. 7. Parameters of this model are determined by fitting the first and second moments, respectively, to the expressions[13]
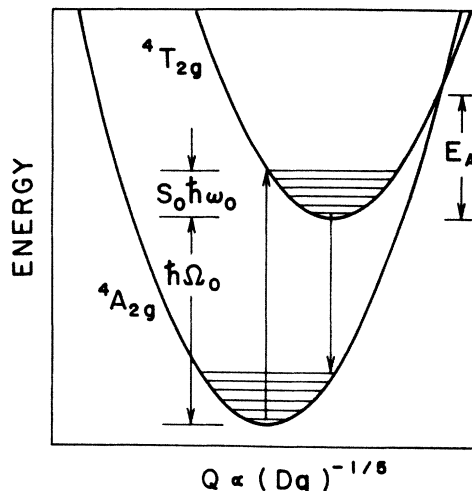

FIG. 7. Adiabatic-potential-energy curves and vibronic energy levels for the single-configuration-coordinate, linear-coupling model. The independent parameters are the zero-temperature Huang-Rhys factor S_0, the phonon energy $\hbar\omega_0$ and the energy gap $\hbar\Omega_0$.

$$N_1 = \hbar\Omega_0 + S_0\hbar\omega_0 \tag{7}$$

and

$$N_2 = S_0(\hbar\omega_0)^2\coth(\hbar\omega_0/2k_BT) . \tag{8}$$

Values of the zero-temperature Huang-Rhys factor S_0, phonon energy $\hbar\omega_0$ and energy gap $\hbar\Omega_0$ (zero-phonon transition energy) are listed in Table III. It is evident from Table III that $\hbar\omega_0$ is significantly less than the phonon energy of the a_{1g} mode derived from resolved vibronic structure of low-temperature spectra.[8,11] It should be regarded instead as an effective phonon energy which incorporates the contributions of both lattice modes and resonances of a_{1g}, e_g, and t_{2g} symmetry in some average way.

The Huang-Rhys factor S_0 is related to the Frank-Condon offset Δ by

TABLE III. Parameters of the single-configuration-coordinate, linear-coupling model (Fig. 7), inferred from the temperature dependence of spectral moments: zero-temperature Huang-Rhys factor S_0, phonon energy $\hbar\omega_0$, and energy gap $\hbar\Omega_0$. The dimensionless quantity R is defined by Eq. (12). The assumed chromium-ligand distance r_0 is one-quarter of the lattice parameter. The curve-crossing energy E_A, defined by Fig. 7, is calculated from Eq. (13). Values inferred from resolved vibronic structure of low-temperature spectra are shown in parentheses for comparison.

	Cs_2NaYCl_6	K_2NaScF_6	K_2NaGaF_6
S_0	6.99	3.95	3.98
$\hbar\omega_0$ (cm^{-1})	228 (300)[a]	380	378 (568)[b]
$\hbar\Omega_0$ (cm^{-1})	11 310 (11 809)[a]	14 280	14 680 (15 041)[b]
r_0(Å)	2.68[c]	2.12	2.06[d]
R	1.89	1.09	0.97
E_A (cm^{-1})	14 810	27 200	28 850

[a]R. W. Schwartz, Inorg. Chem. 15, 2817 (1976).
[b]J. Ferguson, H. J. Guggenheim, and D. L. Wood, J. Chem. Phys. 54, 504 (1971).
[c]L. R. Morse, M. Siegal, L. Stenger, and M. Edelstein, Inorg. Chem. 9, 1771 (1970).
[d]K. Knox and D. W. Mitchell, J. Inorg. Nucl. Chem. 21, 253 (1961).

$$S_0 = M\omega_0\Delta^2/2\hbar . \tag{9}$$

The effective mass M may be identified with the mass of a single halogen ion if the chromium-ligand distance is assumed to be $Q/\sqrt{6}$. One can plot the energy levels of Fig. 1 as functions of Q, provided that the dependence of Dq on Q is known. The elastic energy associated with displacements from the equilibrium configuration Q_0 must be added in order to obtain the adiabatic-potential-energy curves. If one assumes that this additional elastic energy is the same for all states and depends quadratically on $Q - Q_0$, and if one further neglects that part of the curvature of the $^4T_{2g}$ adiabatic-potential-energy curve which is introduced by the transformation from Dq to Q, then linear coupling is preserved and only the effective phonon energy $\hbar\omega_0$ is required in order to complete the configuration-coordinate diagram. The substantial Frank-Condon offset of the $^4T_{2g}$ state is a direct consequence of crystal-field splitting. The slope of the $^4T_{2g}$ adiabatic-potential-energy curve at $Q = Q_0$, the equilibrium position in the $^4A_{2g}$ state,

$$\frac{dE}{dQ} = -M\omega_0^2\Delta , \tag{10}$$

is determined by the crystal-field splitting 10 Dq of the $^4T_{2g}$ and $^4A_{2g}$ states, shown in Fig. 1. With the assumption of a point-charge crystal-field model, $Dq \propto Q^{-5}$, the slope is given by

$$\frac{dE}{dQ} = -50 \, Dq_0/Q_0 . \tag{11}$$

Equations (9)—(11) imply the relation $R = 1$, where R is defined by

$$R = 6Mr_0^2\hbar\omega_0^3 S_0/1250(Dq_0)^2 \tag{12}$$

and $r_0 = Q_0/\sqrt{6}$ is the chromium-ligand distance. In order to test the internal consistency of the various assumptions, values of R have been calculated from the empirical parameters of Tables II and III with r_0 taken to be one-quarter of the host-crystal lattice parameter for want of more precise information. It can be seen that the values of R listed in Table III are satisfactorily close to unity for the fluorides, but not so close for the chloride.

For linear coupling, the energy differences between the intersection of adiabatic-potential-energy curves and the minimum of the upper curve, E_A, is given by

$$E_A = (\hbar\Omega_0 - S\hbar\omega_0)^2/4S\hbar\omega_0 . \tag{13}$$

The energy E_A, which is also listed in Table III, is identified with the activation energy for radiationless transitions in the Mott theory.[15,16] (Inadequacies of the Mott theory are addressed in the context of a more comprehensive theory in II.) A comparison of the values of E_A listed in Table III with the activation energies ΔE of Table I reveals a correct qualitative trend, but a gross quantitative disparity. In fact, Eq. (3) with $s = 10^{13}$ sec^{-1} and $\Delta E = E_A$ fails by about 20 orders of magnitude to explain the observed values of τ_{NR}^{-1}. Stated differently, the measured values of ΔE are much smaller than any relevant features of the configuration-coordinate diagram. Thus the mechanism of fluorescence quenching in low-field chromium complexes cannot be explained in terms of the Mott theory with parameters derived from a single-configuration-coordinate, linear-coupling model. The failure of this theory provides a point of departure for the more comprehensive theory presented in II.

A related investigation of a similar material $(Cs_2NaScCl_6:Cr^{3+})$ has been reported by Strek et al.[17] However, these authors have recorded only the low-temperature portion of the lifetime curve, from which they have attempted to extract a radiationless transition rate. Thus their interpretation of the lifetime data is fundamentally at variance with that of the present work.

ACKNOWLEDGMENTS

*Present address: Department of Chemistry, Boston University, Boston, MA 02215.

†Present address: Department of Chemistry, Harvard University, Cambridge, MA 02138.

[1]H. L. Schläfer, H. Gausmann, and H. Witzke, J. Chem. Phys. **46**, 1423 (1967).

[2]S. Sugano, Y. Tanabe, and H. Kamimura, *Multiplets of Transition-Metal Ions in Crystals* (Academic, New York, 1970), p. 109.

[3]P. T. Kenyon, L. Andrews, B. McCollum, and A. Lempicki, IEEE J. Quantum Electron. QE-18, 1189 (1982).

[4]L. J. Andrews, A. Lempicki, and B. C. McCollum, J. Chem. Phys. **74**, 5526 (1981).

[5]P. F. Moulton and R. E. Fahey, Lincoln Laboratory, M. I. T., Report No. ESD-TR-83-001, 1983 (unpublished).

[6]R. H. Bartram, J. C. Charpie, L. J. Andrews, and A. Lempicki, Phys. Rev. B **34**, 2741 (1986).

[7]S. Desjardins (private communication).

[8]R. W. Schwartz, Inorg. Chem. **15**, 2817 (1976).

[9]H. V. Güdel and T. R. Snellgrove, Inorg. Chem. **17**, 1617 (1978).

[10]D. L. Wood, J. Ferguson, K. Knox, and J. F. Dillon, Jr., J. Chem. Phys. **39**, 890 (1963).

[11]J. Ferguson, H. J. Guggenheim, and D. L. Wood, J. Chem. Phys. **54**, 504 (1971).

[12]P. Greenough and A. G. Paulusz, J. Chem. Phys. **70**, 1967

(1979).

[13]M. Lax, J. Chem. Phys. **20**, 1752 (1952).

[14]P. Giesecke, W. Von der Osten, and U. Röder, Phys. Status Solidi B **51**, 723 (1972).

[15]N. F. Mott, Proc. R. Soc. London, Ser. A **167**, 384 (1938).

[16]R. W. Gurney and N. F. Mott, Trans. Faraday Soc. **35**, 69 (1939).

[17]W. Strek, E. Lukowiak, J. Hanuza, E. Mugenski, R. Cywinski, and B. Jezowska-Trzebiatowska, Physica (Utrecht) **128C**, 259 (1985).